SOME AERODYNAMIC MECHANISMS OF IMPULSIVE NOISE DURING BLADE-VORTEX-INTERACTION

Prof. Dr.-Ing J. Ballmann
Dipl.-Ing. C.S. Kocaaydin
Lehr- und Forschungsgebiet Mechanik der RWTH Aachen
Aachen, West-Germany

Abstract

A computational study of the two-dimensional blade-vortex-interaction was done in comparison to the recent experimental results, which were obtained by wind tunnel and shock tube experiments. The free stream Mach number was varied from the low subsonic to the high transonic regime. Other parameters of interest were the strength, the core radius and the path of vortex, the angle of attack and the thickness of airfoil. Two major aerodynamic mechanisms, which can generate strong acoustic waves were identified in the nearfield. According to the experiments, a critical Mach number related to a transient supersonic pocket on the windward side of the airfoil could be a dominant parameter for the aeroacoustics of helicopters in operation.

Notation

C_L	lift coefficient
C_p	pressure coefficient
e	total specific energy
J	Jacobian
M_∞	free stream Mach number
p	pressure
r_0	radius of vortex core
t	dimensionless time
U_∞	free stream velocity
u, v	velocity components
v_ϑ	vortex induced velocity
x, y	dimensionless cartesian coordinates
x_V, y_V	dimensionless vortex location
$\bar{\Gamma} = \frac{\Gamma}{U_\infty C}$	dimensionless vortex strength
$\nu^* = \frac{C}{y_V}$	frequency
ρ	mass density
ξ, η	curvilinear coordinates

1. Introduction

It has been generally accepted and experimentally validated, that one of the major sources of helicopter noise is due to the blade-vortex-interaction (BVI), e.g. Ref 1. The special case of parallel vortex axis and blade is considered to be the most intense acoustic source. According to the knowledge of the authors, this special two-dimensional case has been successfully realised in two-dimensional shock tube and wind tunnel experimental setups for the first time by G.E.A. Meier at Göttingen (Ref 2-4 and Fig 1-2). For a clockwise rotating vortex passing the underside of a profile these experiments have demonstrated that there are two basic aerodynamic mechanisms for the development of strong acoustic waves:

i- Rapid dislocation of the stagnation point at the leading edge causes an upstream moving compression wave.

ii- The collapse of transient local supersonic pockets attached at the airfoil generates an upstream propagating weak shock wave.

Another result of the experimental studies is that the leading edge region of the airfoil seems to be the most important part of the flow field. It is assumed that the chord length is not a dominant parameter.

Valuable informations about the vortex structure in shock tube experiments have been given by Bershader, who has done similar shock tube experiments (Ref 5). The measured density field inside the vortex core has been used to determine the vortex strength, while making some assumptions on the thermodynamic state.

The numerical simulation of blade-vortex-interaction has attracted a lot of researchers, who have used different models with varying degrees of complicacy. Several models ranging from linear potential theory over transonic small disturbance theory to thin layer Navier-Stokes equations have been used (Ref 6). The simple methods based on linear potential theory are actually very helpful to get an idea about the distortion of vortical fields, because of the Lagrangean nature of vortex convection in these schemes.

2. Numerical Aspects

The numerical simulation of blade-vortex-interaction is considered as a complicated aeroacoustic problem, which needs careful interpretation of numerical solutions. Several authors have contributed to the understanding of this phenomena (e.g. Ref 6-10).

There are three major numerical aspects of the problem,

i) resolution of transonic effects,
ii) convection and distortion of vortices and vortical flow fields,
iii) propagation of acoustic waves.

Upwind finite difference methods have reached nowadays a satisfactory level, so that transonic flow regimes can be investigated. In this case special interest is on the shock-capturing capability of the numerical scheme, so that unsteady shock wave behaviour on airfoils can be described completely.

On the other hand finite difference schemes possess enough artifical viscosity, so that the vortical flow fields are smeared and distorted very rapidly. The vortex-capturing capability of the schemes is still in development. It is generally accepted that the coarser the finite difference grid is that is used to perform the computation, the greater the distortion of the vortex is. This is completely a numerical dissipation process. In order to perform an accurate BVI simulation an extra fine grid would have to extend all the way through the vortex passing field.

There have been two major contributions concerning these aspects of the problem. A perturbation approach has been introduced to handle weak interactions more accurately (Ref 7), where known properties of the vortex structure can be used to generate source terms in the governing equations that counteract the effect of artifical dissipation of the numerical scheme.

The other contribution is the development of higher-order upwind schemes with low numerical dissipation (Ref 11, 12). It has been also possible to keep the travelling vortex stable, where a zonal grid was used.

The resolution of propagating acoustic waves has been possible only through a smooth grid spacing and fine grid in the farfield of the airfoil.

3. Solution Procedure

The mathematical model of the two-dimensional problem, see Fig 3 is based on the Euler equations, while viscous effects are neglected.

As far as the aerodynamic generation of sound waves is concerned this assumption is fully justified. On the other hand, the vortex should also be modelled in the same manner. So the details of the vortex' viscous core cannot be described. This leads inevitably to a physically diffusion-free vortex model. Therefore it will be appropriate to consider only weak and medium interactions.

Actually there isn't any published work, where the viscous structure of the vortex has been fully taken into account for BVI. Even in Navier-Stokes computations, the insertion of the vortex into the computational domain is similar as for simulations neglecting viscosity.

It is especially desirable to use the strong conservation form of Euler equations for numerical computations if an upwind finite difference scheme is applied.

$$\frac{\partial \mathfrak{Q}}{\partial t} + \frac{\partial \mathfrak{F}(Q)}{\partial \xi} + \frac{\partial \mathfrak{G}(Q)}{\partial \eta} = 0 \ ,$$

$$\mathfrak{Q} = \frac{1}{J} (\rho, \rho u, \rho v, e)^T \ ,$$

$$\mathfrak{F}(Q) = \frac{1}{J} (\rho \hat{U}, \rho u \hat{U} + \xi_x p, \rho v \hat{U} + \xi_y p, \hat{U}(e+p))^T,$$

$$\mathfrak{G}(Q) = \frac{1}{J} (\rho \hat{V}, \rho u \hat{V} + \eta_x p, \rho v \hat{V} + \eta_y p, \hat{V}(e+p))^T,$$

$$\hat{U} = \xi_x u + \xi_y v \quad , \quad \hat{V} = \eta_x u + \eta_y v \ ,$$

$$J = \xi_x \eta_y - \xi_y \eta_x = (x_\xi y_\eta - x_\eta y_\xi)^{-1} \ .$$

An explicit scheme has been applied to integrate the Euler equations in a time-accurate manner. The basic method is a one-dimensional upwind scheme with an integrated Riemann solver of Roe-type, where a two-step MUSCL-type formulation is used to enhance the order of time accuracy. This scheme has been implemented for the two-dimensional system by using the Strang-type of fractional-step method. Details of numerical scheme are not given here, they can be found in Ref 13-14.

The domain of the numerical solution reaches from x=-6 to x=3 with the origin at the leading edge of the profile. Before entering to the solution domain (see Fig 4), the vortex is assumed to be of Lamb type, taking into account compressibility; its strength, velocity distribution and coordinate y_v are kept fixed. Thereafter the vortex is set free and its vorticity field becomes part of the numerical solution.

The computation is initialized with a steady state full potential solution past the profile without the vortex. Than the vortex is set into the flow at a point far upstream of the solution domain. From the beginning the conditions at the artificial boundary of the domain of numerical solution are adjusted with time to include the additional mass transfer induced by the travelling vortex. The procedure is similar to that in Ref 12.

For the numerical treatment of the Euler equations we used two

approaches, i.e. the perturbation approach of G.R. Srinivasan et al. (Ref 7) and the Euler equations without any decomposition.

Test runs of the numerical algorithm were carried out to improve the preserving of the vortex structure and the correct simulation of vortex shock interaction which is essential for the interference of a vortex crossing a transonic shock.

4. Parameters

The parameters of the inviscid model are the vortex strength Γ, the radius r_0 of the vortex core, the vertical misalignment y_V of the approaching vortex, the free stream Mach number M_∞, the chord length C and the airfoil shape parameters. As far as possible the parameters of the compressible Lamb type vortex were taken from experiments of G.E.A. Meier and his group. It is usual to define a reduced frequency ν^* from the given parameters, $\nu^* := C/y_V$. In the parameter range of interest is $y_V < C$, so that $\nu^* > 1$. This is a rough estimation that the BVI is a very strong unsteady process. The characteristic length scale of the given parameters can be arranged as $r_0 < y_V < C$.

In order to get an idea about the vortex strength, it could be compared with the airfoil lift. According to the potential theory, the lift coefficient C_L of an airfoil having circulation Γ is given by $C_L = 2\Gamma/U_\infty C$. So it is appropriate to define a non-dimensionalized vortex strength parameter $\bar{\Gamma} = \Gamma/U_\infty C$. It is important to note the unsteady nature of the problem at this point. The airfoil interacting with a vortex having strength Γ can attain only a fraction of related steady state lift $C_L = 2\Gamma/U_\infty C$ for also a very short time.

5. Results

Two direct comparisons of computational and experimental results with clockwise rotating vortices are presented in Fig 5 and 6. Fig 5 is related to a wind tunnel experiment with a lifting profile (SC 1095) and a vortex generator producing a vortex street. To reduce the interaction of the vortices the vortex street is streched by a subsequently added Laval-nozzle. The vortex parameters were $M_\infty = 0.73$, $\bar{\Gamma} = 0.42$, $r_0 = 0.1$, $y_V = -0.31$ and, since the data of the other profile were not available, the computation was carried out for the NACA 2209 profile which has a similar geometry . The results are in good agreement as long as the disturbances induced by the next vortex of the impinging vortex street are still weak.

Fig 6 contains the direct comparison with a shock tube experiment. The parameters are $M_\infty = 0.57$, dimensionsless vortex strength $\bar{\Gamma} = 1.8$, initial vortex misalignment $y_V = -0.31$, vortex core radius $r_0 = 0.1$.

A strong distortion of the vortex, the generation of a supersonic pocket on the lower side of the airfoil, the propagation of a compressibility wave and a transonic shock wave have been observed in the experiment and also verified in the numerical computations.

When the vortex approaches the airfoil, the flow on the upper side is decelerated and the stagnation point is shifted to this side. On the lower side the flow is accelerated. The vortex is strong enough to produce a supersonic pocket attached at the lower surface

of the profile and closed by a transonic shock wave. Firstly the supersonic region grows up and the shock moves downstream becoming stronger. When the vortex passes the leading edge, the downwash diminishes rapidly and an upwash is induced. The situation is similar to that of an airfoil undergoing an instantaneous and strong change in its angle of attack. In order to adjust to the new flow conditions, the stagnation point moves towards the lower side. The flow on the upper side begins to accelerate and a compressibility wave is observed propagating upstream. The vortex crossing the supersonic pocket under the airfoil, intensifies the shock wave, which moves still backwards. Finally the vortex overtakes the shock wave. Afterwards the supersonic domain starts to shrink and the shock wave changes simultaneously its moving direction. The shock propagates upstream beeing weakened. The fact that the relative velocity of the oncoming flow with respect to the upstream moving shock wave remains supersonic, enables its propagation. The supersonic pocket is completly collapsed when the shock arrives at the leading edge and is radiated upstream as a pressure wave which may contribute to the impulsive noise as well as the compression wave.

During the passage of the vortex at the leading edge with its sudden change of the effective angle of attack, the vorticity shed from the trailing edge will change its sign. This phenomenon will result in an accumulation of negative vorticity at the profile. The experiments show the same change of sign of the resulting vorticity. The overall agreement between experimental and computational results seems to be sufficient.

As the vortex passes the trailing edge, a compression wave is induced on the upper side due to the deflection of the wake by the vortex. For flows with higher free-stream Mach numbers this upstream running compression wave may steepen to a shock wave. this happened e.g. in a numerical simulation with M_∞=0.72 for a profile NACA 0012, see the middle row of diagrams in Fig 7. Reaching the leading edge this shocklet becomes an upstream running compression wave which may be recorded by the observer A as the third pressure pulse, see the above diagram in the middle row of Fig 8. The first and the second pressure pulse registrated at point A originate at the interaction of the vortex with the leading edge (the so-called compression wave) and with the lower side of the airfoil.

Computional results which were realized for the profile NACA 0012 at two other Mach numbers but with the same values of the vortex parameters ($\bar{\Gamma}$=0.4, r_0 = 0.15, y_V = -0.3) are also presented in Fig 7-9. The different rows of diagrams belong to the different Mach numbers.

Fig 7 shows the pressure fluctuations, Fig 8 the vortex path together with the streamlines of the undisturbed steady flow and the pressure signals recorded with time by two observers located at the points A and B. Fig 9 shall demonstrate the development and propagation of radiated pressure waves running upstream. A and B are at rest in the reference frame fixed with the profile.

For M_∞=0.63 the pressure fluctuations induced by the passing vortex at the lower and the upper side remain relatively weak, compared with the

results for higher Mach numbers. This corresponds to the fact that only weak compression waves are radiated upstream and recorded by the observers A and B, marked in the first row of figure O. The different compression waves are staggered, corresponding to their different times of development. Like in the case of M_∞=0.73, the first wave forms when the vortex passes by the leading edge, the second originates from the interaction with the lower side of the profile and the third comes from the upper side, originated by the interference with the trailing edge. This corresponds to the different pressure rises observed at the points A and B. Each signal has his highest amount at the side where it comes from.

With higher Mach numbers the pressure signals become stronger, according to earlier results given in Ref 8. As already mentioned above for M_∞=0.73, in a flow which is purely subsonic without the vortex, transient supersonic pockets may occur, first at the lower side and later at the upper side.

Looking at the case of the Mach number M_∞=0.81, supersonic pockets exist already in the undisturbed flow without the vortex. In this case the shock on the lower side undergoes a very strong interaction with the vortex but the observed pressure rises were not very much higher than for M_∞=0.73.

Vortex trajectories show a substantial deviation from simple convection along the streamlines of the stationary flow around the airfoil without the vortex, as can be seem from Fig 8. In fact the vortex path shows a highly nonlinear dependence on the airfoil lift, the strength and the initial position of the vortex. The temporal change of lift indicates that at the beginning of the interaction, the shed wake is weak. However, when the vortex passes the trailing edge, the shed vorticity becomes stronger. After the vortex has passed the trailing edge at a narrow distance, a strong interaction with the wake is to be expected. This can result in wake-roll-up, depending on the sign and strength of the two vortex fields. Some kind of merging with the wake vorticity appears to be taking place after the vortex has traveled two chord lengths past the trailing-edge. Bearing in mind that the vortex core is about 30% of the chord, its actual path will lie in a band around the computed mean location.

6. Concluding Remarks

Distortion of the vortical structure incident on the leading-edge seems to be limited to a domain which is less than the characteristic vortex diameter upstream the airfoil. It is expected, that details of the vortex distortion during the interaction should not substantially influence the path of the vortex, if it is not splitted severely.

Secondary vortex generation in the boundary layer has been observed in the experiments, which influences the vortex trajectory in a substantial manner.

This physical process has been identified to be the result of boundary layer separation behind a forward traveling shock wave under the airfoil. Initially a separation bubble is generated at the root of the shock-wave. As long as the shock wave was moving downstream, this separation bubble could not grow. After the shock-vortex interaction, a massive separation may

occur.The vorticity shed into flow interacts with the primary vortex. The counterrotating secondary vortex and the primary vortex merge finally.

Finally it should be marked that, depending on the parameters, all types of unsteady transonic shock phenomena classified in Ref 15 could be observed in the computations: transient appearence of transonic shocks in a formerly undisturbed subsonic flow, transient disappearence of transonic shocks in a formerly undisturbed transonic flow and motions of transonic shocks. As already found out in Ref 8, in all cases the vortex appears as the center of disturbance. This fact is physically reasonable since the vortex moves approximately according to the Kelvin-Helmholtz-law with the fluid, i.e. with the medium of wave propagation. In conrtary to Ref 10 the vortex showed no signs of a bow wave of itself, neither in the experiments nor in the computations.

7.Acknowledgements

The authors thank Dr. G.E.A. Meier and his group for experimental data and fruitful cooperation. Furthermore the financial support of the Deutsche Forschungsgemeinschaft is gratefully acknowledged.

Literature

1. SCHMITZ, F.H. and YU, Y.H. Helicopter Impulsive Noise: Theoretical and Experimental Status, In: Krothapelli, A., Smith, C.A., (Ed.) Recent Advances in Aeroacoustics, Berlin, Heidelberg, New York, Springer, 1986

2. MEIER, G.E.A. and TIMM, R. Unsteady Vortex Airfoil Interaction. Report of the Max-Planck-Institut für Strömungsforschung, Göttingen, 1986

3. MEIER, G.E.A., LENT, H.-M. and LÖHR, K.F. Sound Generation and Flow Interaction of Vortices with an Airfoil and a Flat plate in Transonic Flow, Fluid Dynamics Research, 1988, **3**, 344-348

4. MEIER, G.E.A., SCHIEVELBUSCH, K. and LENT, H.-M. Stoßwellen-entstehung bei transsonischer Wirbel-Profil-Wechselwirkung, submitted to ZWF, 1989

5. BERSHADER, D. Shock Tube Studies of Vortex Structure and Behaviour, in: Grönig, H., (Ed.) Proc. of the Sixteenth International Symposium on Shock Tubes and Waves, Aachen, July 1987, Weinheim, VCH, 1988

6. CARADONNA, F.X. The Application of CFD to Rotary Wing Flow Problems. AGARD-FDP-VKI Special Course on Aerodynamics of Rotorcraft, 1990

7. SRINIVASAN, G.R., MCCROSKEY, W.J. and BAEDER, J.D. Aero-dynamics of Two-Dimensioal Blade-Vortex Interaction, AIAA J., 1986, **24**, 1569-1576

8. BAEDER, J.D., MCCROSKEY, W.J. and SRINIVASAN, G.R. Acoustic Propagation Using Computational Fluid Dynamics. Proc. of the 42th Annual Forum of the American Helicopter Society, Vol. 1, Washington, D.C., 1986, 551-562

9. SRINIVASAN, G.R. and MCCROSKEY, W.J. Numerical Simulation of Unsteady Airfoil-Vortex Interactions. Vertica, 1987, **11**, 3-28

10. GEORGE, A.R. and LYRINTZIS, A.S. Acoustics of Transonic Blade-Vortex Interactions, AIAA J., 1988, **26**, 769-776

11. MUNZ, C.-D. On the Comparison and Construction of Two-Step Schemes for the Euler Equations, in: Notes on Numerical Fluid Mechanics, 14, Hirschel, E.H., (Ed.), Braunschweig, 1986

12. RAI,M.M. Navier-Stokes Simulations of Blade-Vortex Interaction Using High-Order Accurate Upwind Schemes. Paper AIAA-87-0943, 1987

13. KOCAAYDIN, C.S. and BALLMANN, J. Wechselwirkung von Wirbeln mit Profilen, submitted to ZFW 1989

14. KOCAAYDIN, C.S. Aerodynamik der Impulsschallentstehung durch Wirbel-Profil- Wechselwirkung, Diss., RWTH Aachen, VDI-Verlag, 1990

15. TIJDEMAN, H. and SEEBASS, R. Transonic Flow Past Oscillating Airfoils, Ann. Rev. Fluid Mech., 1980, **12**, 181-222

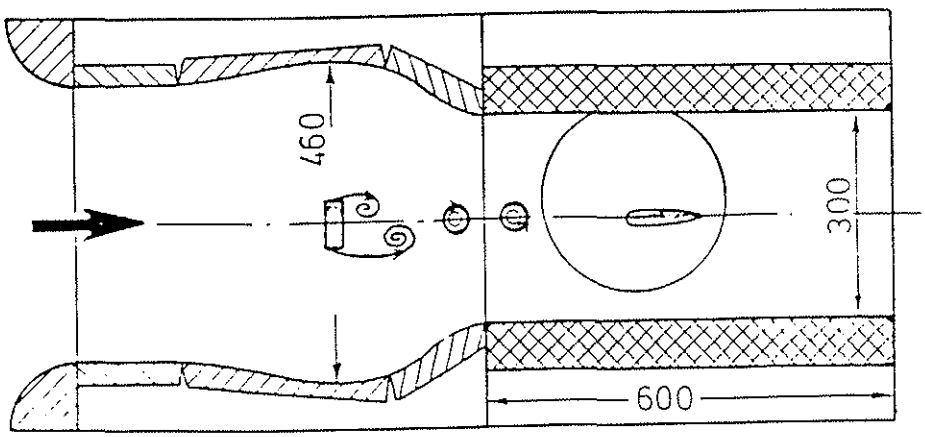

Fig 1. Setup in the wind tunnel experiments. The decrease of the cross-sectional area accelerates the flow and the vortex distance.

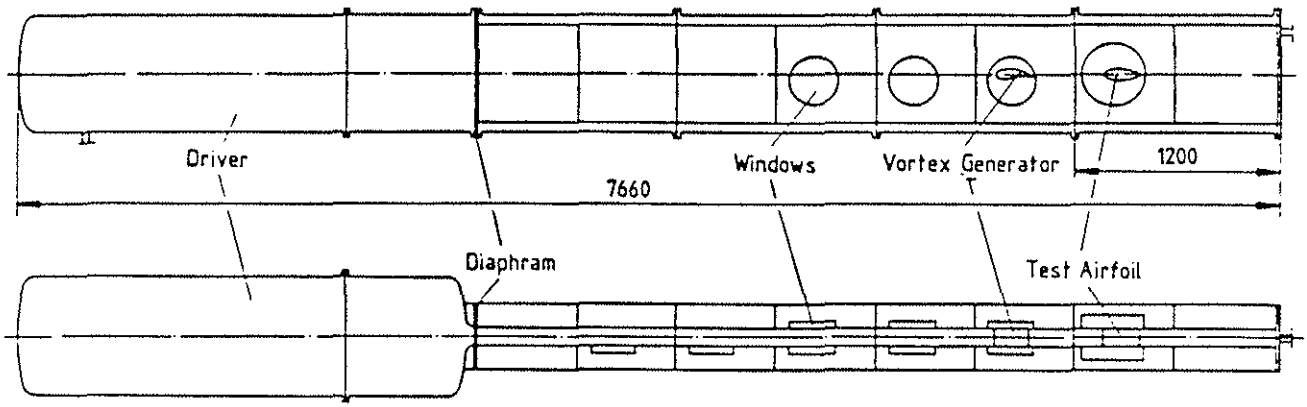

Fig 2. Setup in the Shock tube experiments. The shock generates the oncoming flow and at the vortex generator a single vortex.

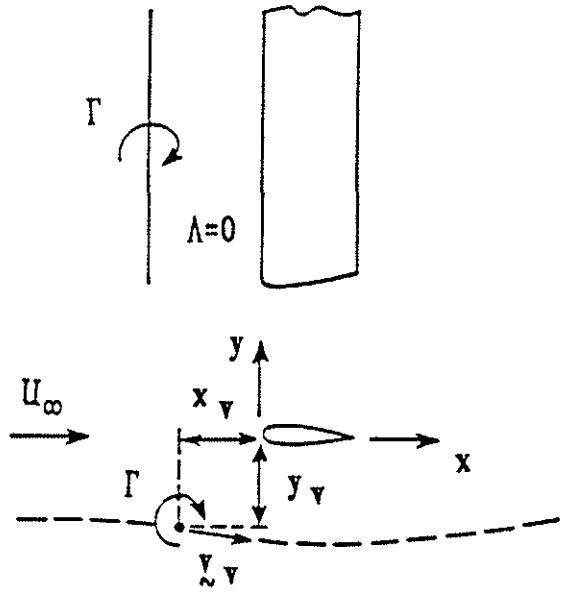

Fig 3. Flow Model

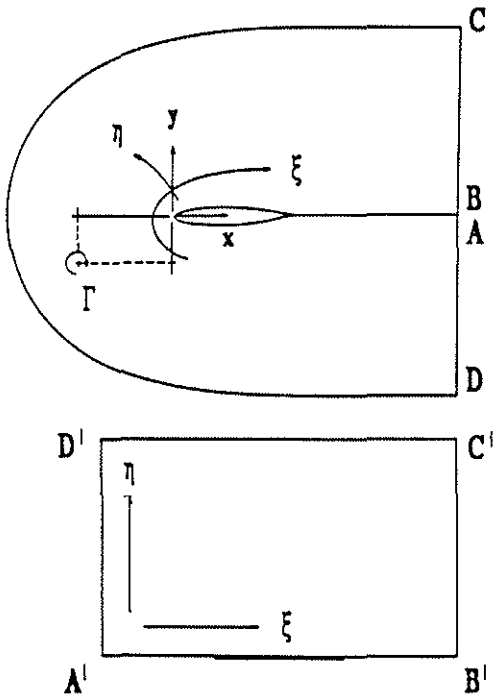

Fig 4. Reference frame

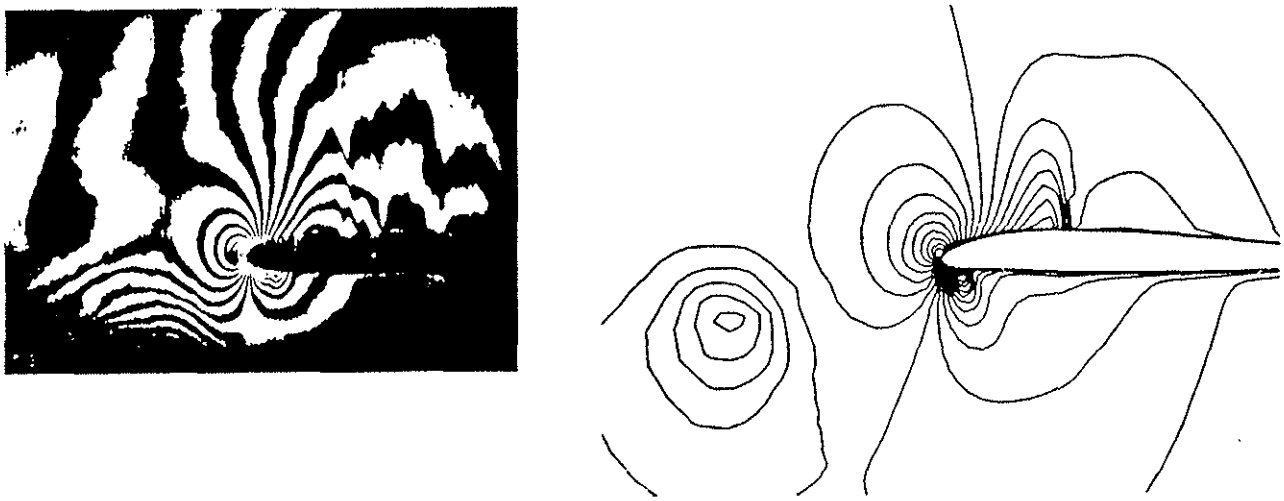

$M_\infty = 0{,}73$

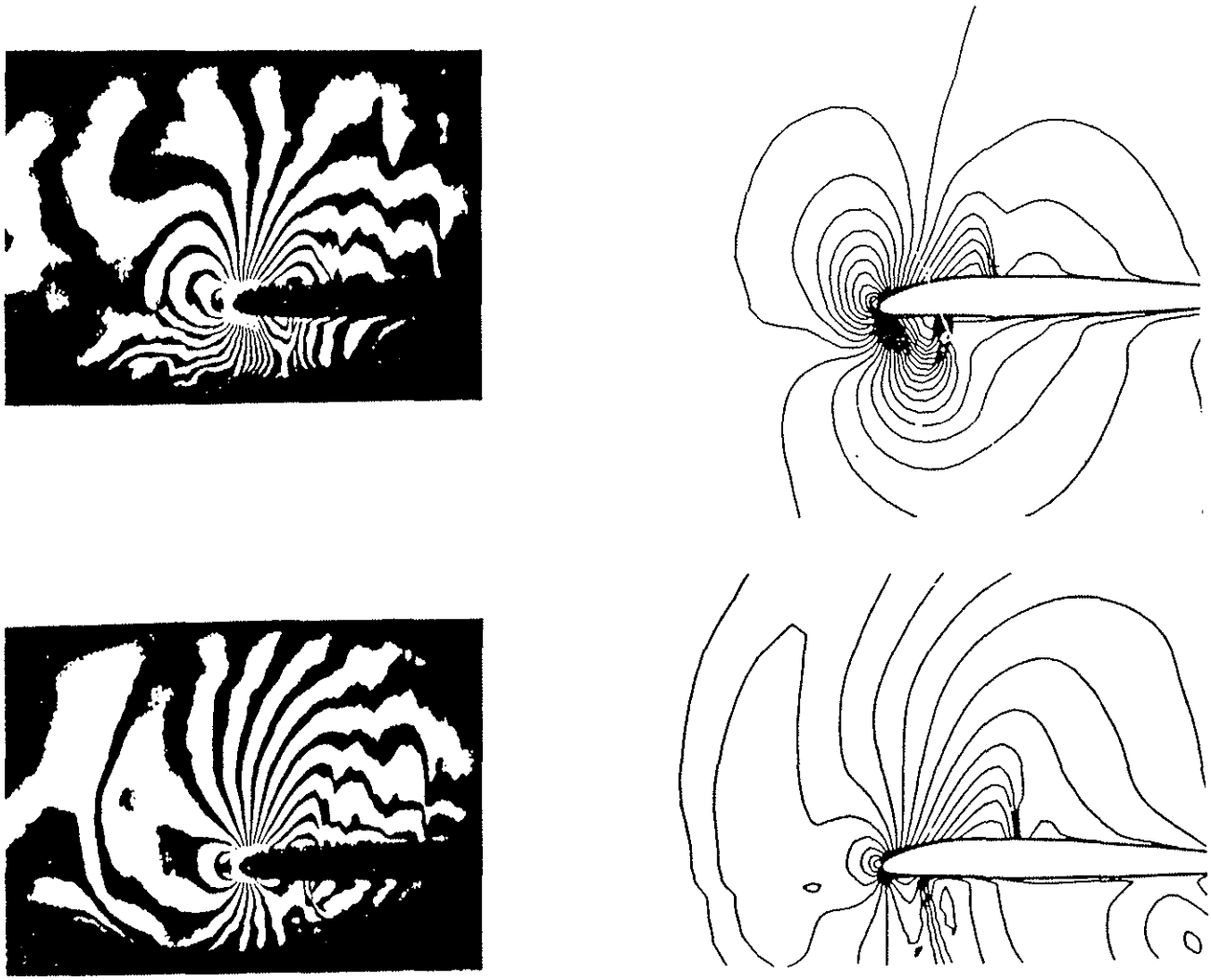

Fig 5. Experimental and computational results for the density contour lines. Wind tunnel experiment with a profile SC 1095. Computation for NACA 2209. Parameters $M_\infty = 0.73$, $\bar{\Gamma} = 0.42$, $r_0 = 0.1$, $y_V = -0.31$

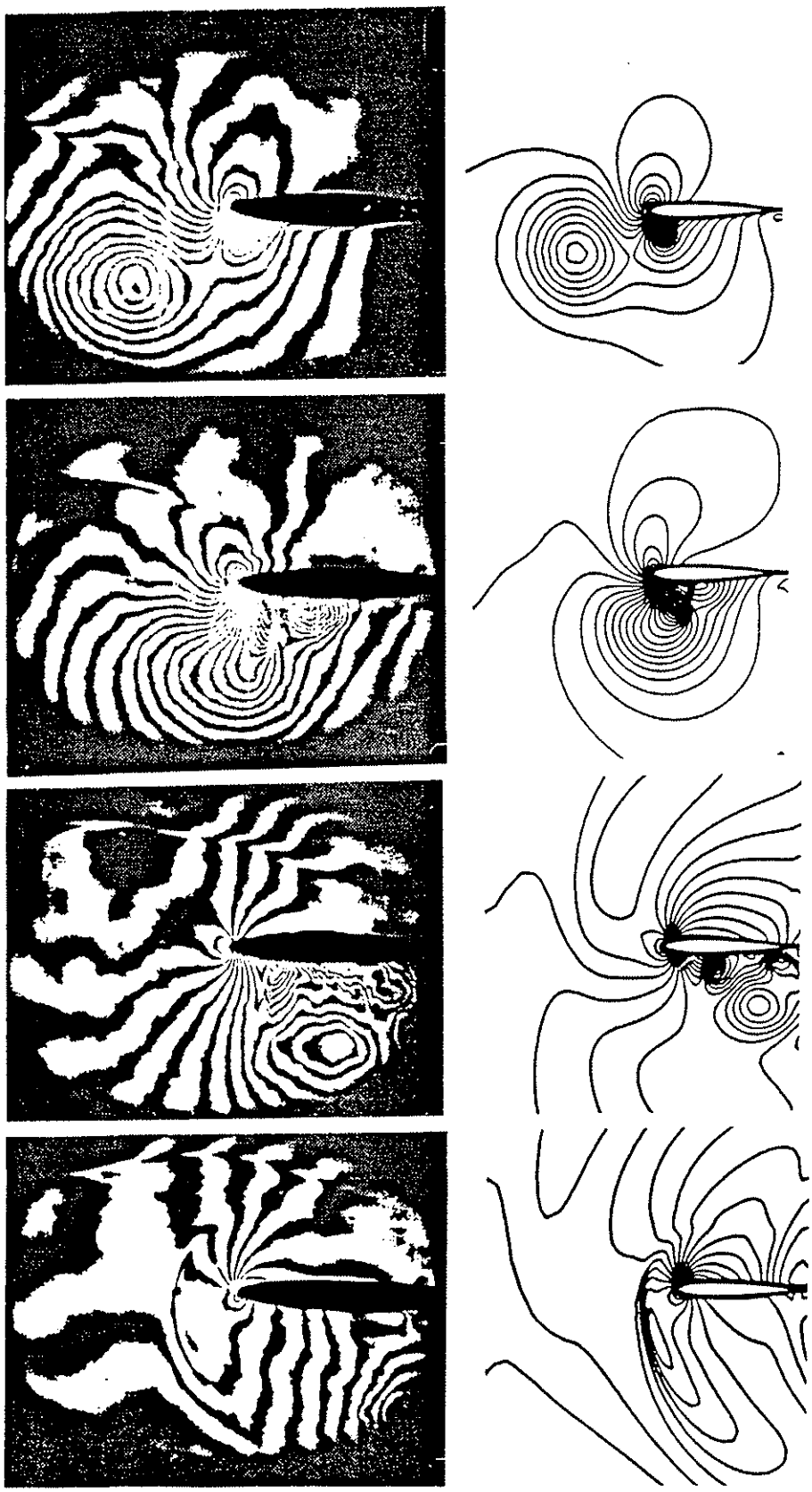

Fig 6. Experimental and computational results for the density contour lines. Shock tube experiment. Profile NACA 0012.
Parameters $M_\infty = 0.57$, $\overline{\Gamma} = 1.8$, $r_0 = 0.1$, $y_V = -0.31$

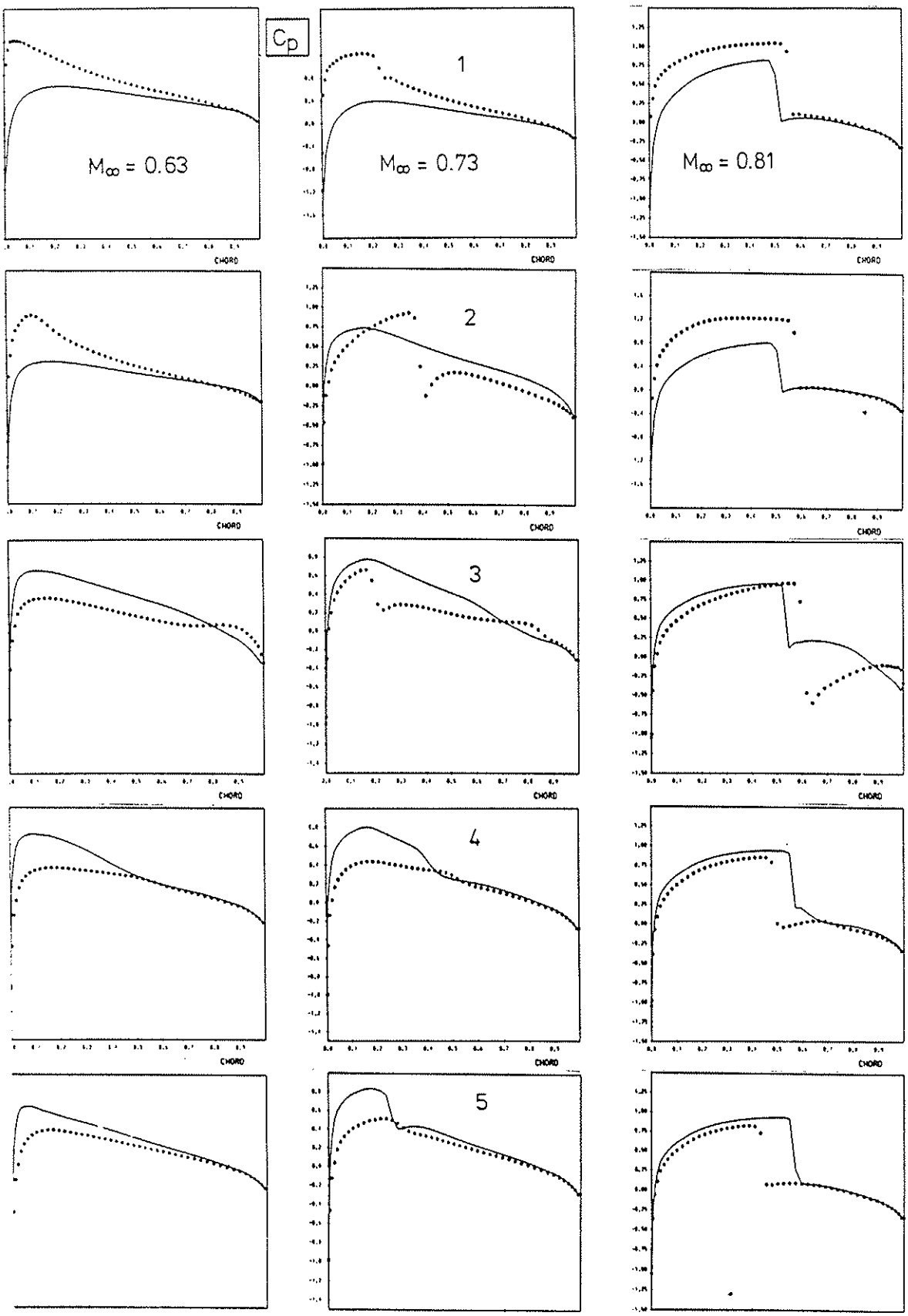

Fig 7. Pressure fluctuation during profile-vortex interaction
Parameters $\bar{\Gamma}$= 0.4, r_0= 0.15, y_V = −0.3

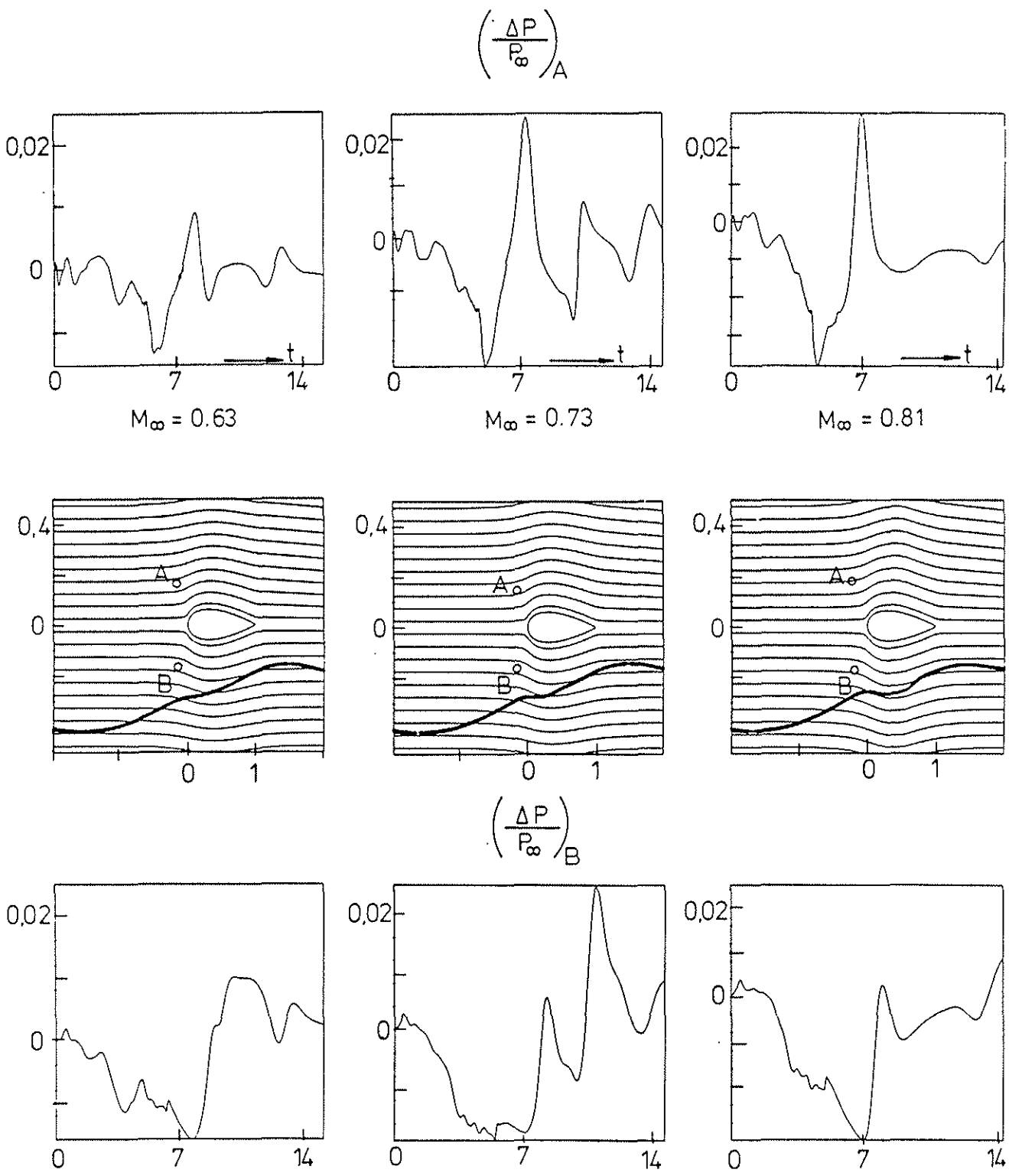

Fig 8. Pressure signals registrated in a reference frame fixed at the profile by observers A and B.
Parameters $\bar{\Gamma}$= 0.4, r_0= 0.15, y_V = -0.3

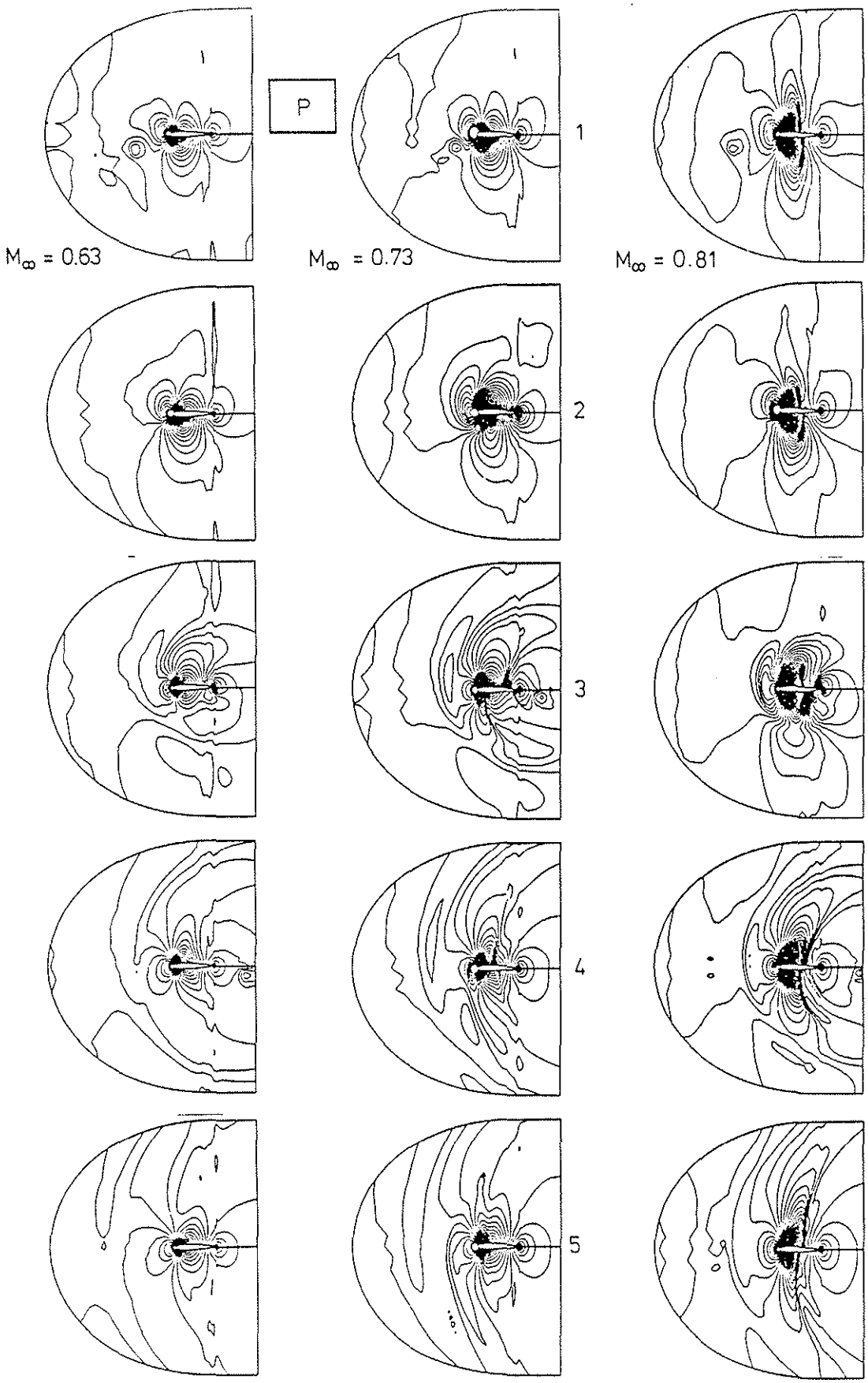

Fig 9. Contourlines of pressure during profile-vortex interaction.
Parameters $\bar{\Gamma}$= 0.4, r_o= 0.15, y_v= -0.3